BBA - Molecular Basis of Disease 1865 (2019) 2048–2059

Contents lists available at ScienceDirect

BBA - Molecular Basis of Disease

journal homepage: www.elsevier.com/locate/bbadis

Diminished *O*-GlcNAcylation in Alzheimer's disease is strongly correlated with mitochondrial anomalies☆

Tiffany S. Pinho[a], Sónia C. Correia[a,*], George Perry[b], António Francisco Ambrósio[c], Paula I. Moreira[a,d,**]

[a] *CNC — Center for Neuroscience and Cell Biology, University of Coimbra, Portugal*
[b] *Department of Biology, University of Texas at San Antonio, TX, USA*
[c] *Coimbra Institute for Clinical and Biomedical Research (iCBR), Faculty of Medicine, University of Coimbra, Portugal*
[d] *Institute of Physiology, Faculty of Medicine, University of Coimbra, Coimbra, Portugal*

ARTICLE INFO

Keywords:
Alzheimer's disease
Human brain tissue
in vitro and *in vivo* Alzheimer's models
Mitochondria
O-GlcNAcylation
Thiamet-G

ABSTRACT

Uncover the initial cause(s) underlying Alzheimer's disease (AD) pathology is imperative for the development of new therapeutic interventions to counteract AD-related symptomatology and neuropathology in a timely manner. The early stages of AD are characterized by a brain hypometabolic state as denoted by faulty glucose uptake and utilization and abnormal mitochondrial function and distribution which, ultimately, culminates in synaptic "starvation" and neuronal degeneration. Importantly, it was recently recognized that the post-translational modification β-*N*-acetylglucosamine (*O*-GlcNAc) modulates mitochondrial function, motility and distribution being proposed to act as a nutrient sensor that links glucose and the metabolic status to neuronal function. Using post-mortem human brain tissue, brain samples from the triple transgenic mouse model of AD (3xTg-AD) and *in vitro* models of AD (differentiated SH-SY5Y cells exposed to AD-mimicking conditions), the present study is aimed to clarify whether *O*-GlcNAcylation, the posttranslational modification of intracellular proteins by *O*-GlcNAc, contributes to "mitochondrial pathology" in AD and its potential as a therapeutic target. A reduction in global *O*-GlcNAcylation levels was observed in the brain cortex and hippocampus of AD subjects. Moreover, GlcNAcylation levels are higher in mature mice but the levels of this posttranslational modification are lower in 3xTg-AD mice when compared to control mice. The *in vitro* models of AD also exhibited a marked reduction in global *O*-GlcNAcylation levels, which was strongly correlated with hampered mitochondrial bioenergetic function, disruption of the mitochondrial network and loss of cell viability. Conversely, the pharmacological modulation of *O*-GlcNAcylation levels with Thiamet-G restored *O*-GlcNAcylation levels and cell viability in the *in vitro* models of AD. Overall, these results suggest that *O*-GlcNAcylation is involved in AD pathology functioning as a potential link between mitochondrial energetic crisis and synaptic and neuronal degeneration. This posttranslational modification represents a promising therapeutic target to tackle this devastating neurodegenerative disease.

1. Introduction

Alzheimer's disease (AD) is the leading cause of dementia in the elderly population, affecting approximately 40 million people worldwide [1,2]. This neurodegenerative disease is the result of progressive neurodegenerative changes in the human brain, which lead to a progressive decline in memory, language and attention [3]. From a neuropathological point of view, the AD brain exhibits the presence of two distinctive pathological hallmarks: the extracellular deposition of amyloid-β (Aβ) peptide in senile plaques and the intracellular accumulation of neurofibrillary tangles (NFTs) composed of hyperphosphorylated tau protein [4]. Additional features include microgliosis and a widespread and progressive loss of neurons, synapses and white matter [1,5]. Cognitive and behavioral symptoms constitute only the

☆ This article is part of a Special Issue entitled: Post-Translational Modifications in Brain Health and Disease edited by Paula Moreira, Susana Cardoso and Sónia Correia.

* Correspondence to: S. C. Correia, Center for Neuroscience and Cell Biology, University of Coimbra, 3004-504 Coimbra, Portugal.
** Correspondence to: P. I. Moreira, Laboratory of Physiology, Faculty of Medicine, University of Coimbra & Center for Neuroscience and Cell Biology, University of Coimbra, Coimbra, Portugal.
E-mail addresses: sonia.correia@cnc.uc.pt (S.C. Correia), venta@ci.uc.pt, pimoreira@fmed.uc.pt (P.I. Moreira).

https://doi.org/10.1016/j.bbadis.2018.10.037
Received 19 August 2018; Received in revised form 25 October 2018; Accepted 29 October 2018
Available online 06 November 2018

"tip of the iceberg", since the disruption of brain structure and function and consequent neuronal loss precede the clinical signs of the disease by 20–30 years [6]. Within this scenario, defective cerebral metabolism has gained attention as a possible initial cause of this neurodegenerative disease, particularly for the sporadic cases of AD, where aging and metabolic disorders are main risk factors [7,8]. In fact, compelling evidence revealed that regional brain hypometabolism occurs prior to the occurrence of senile plaques and NFTs in both genetic and sporadic AD [9–14] suggesting impaired glucose metabolism may be an upstream event in AD progression.

The nutrient-sensing pathway that encompasses the dynamic and reversible post-translational modification called *O*-linked-β-*N*-acetylglucosaminylation (*O*-GlcNAcylation) plays a significant role in disease progression. In fact, *O*-GlcNAcylation of nuclear, cytoplasmic and mitochondrial target proteins is proposed to act as a metabolic sensor that links glucose metabolism to neuronal function. In a process that resembles phosphorylation [15], *O*-GlcNAc, derived from the final product of the nutrient-dependent hexosamine biosynthetic pathway (HBP), is added to or removed from hydroxyl groups of serine and/or threonine residues by two highly conserved intracellular enzymes, *O*-GlcNAc transferase (OGT) and O-linked-β-*N*-acetylglucosaminidase (OGA), respectively [16,17].

Recent breakthroughs revealed that the forebrain-specific loss of OGT in adult mice leads to progressive neurodegeneration, accumulation of protein aggregates and memory deficits [18]. Moreover, amyloid precursor protein (APP) and tau protein, as well as several proteins involved in regulatory cascades that mediate intracellular signaling, were shown to be heavily modified by *O*-GlcNAc [19].

During synaptic activity *O*-GlcNAcylation also regulates mitochondrial trafficking by targeting the mitochondrial motor-adaptor Milton, which is responsible for tethering mitochondria to motor proteins allowing the movement of these organelles along the microtubule tracks [20]. However, so far, there is no consensus regarding the exact participation of *O*-GlcNAcylation in AD with conflicting data reporting both augmented and diminished *O*-GlcNAcylation levels in this neurodegenerative disease. Furthermore, the exact mechanism responsible for altered *O*-GlcNAcylation in AD brain remains inconclusive.

Taking into account that AD-related glucose hypometabolism is accompanied by an abnormal mitochondrial function and distribution within neurons, which ultimately culminates in synaptic "starvation" and neuronal degeneration, and that *O*-GlcNAcylation was shown to modulate mitochondrial function, motility and distribution, the present study was undertaken to clarify the involvement *O*-GlcNAcylation in AD mitochondrial pathology.

2. Materials and methods

2.1. Chemicals

Streptozotocin (STZ) was obtained from Sigma (CAS 18883-66-4), the synthetic Aβ1–42 peptide was purchased from Bachem (CAS 4014447), okadaic acid (OA) was acquired from Calbiochem (CAS 78111-17-8) and Thiamet-G purchased at Cayman Chemical (CAS 1009816-48-1). Antibodies were obtained from the following sources: Anti-actin (1:5000, mouse, A5441 Sigma); O-Linked N-Acetylglucosamine antibody — RL2 (1:1000, mouse ab2739 Abcam); Anti-TOM20 (1:200, rabbit, sc-11415 Santa Cruz Biotechnology); ECL anti-mouse IgG horseradish peroxidase (HRP) conjugate (1:10,000, goat, NA931-1ML GE Healthcare Life Sciences); ECL anti-rabbit IgG horseradish peroxidase (HRP) conjugate (1:10,000, donkey, NA934-1ML GE Healthcare Life Sciences); Alexa Fluor 488 anti-rabbit IgG conjugate (1:100, goat, A11008 Life technologies); Alexa Fluor 594 anti-mouse IgG conjugated (1:100, goat, A11005 Life technologies). All the other chemicals were of the highest grade of purity commercially available.

Table 1
Age and post-mortem intervals of subjects with histopathologically confirmed AD and aged-matched controls.

	Age	PMI
Control 1	74	8
Control 2	68	2.5
Control 3	66	4
Control 4	84	5
Control 5	83	2
Control 6	86	4
Control 7	74	6
Control 8	92	4.5
AD 1	83	6
AD 2	79	8
AD 3	84	4
AD 4	85	9
AD 5	80	5.5
AD 6	83	4
AD 7	78	5
AD 8	66	12
AD 9	65	6
AD 10	94	12
AD 11	78	5

AD — Alzheimer's disease; PMI — post-mortem interval.

2.2. Human brain tissue

Hippocampal and brain cortical tissue samples were obtained at autopsy from subjects with histopathologically confirmed AD and aged-matched controls (Table 1).

2.3. Animals

Hippocampal and brain cortical tissue samples from 6 to 8 and 11–12-month-old male wild type (WT; C57BL6/129S) and 3xTg-AD mice were used. Animals were bred and maintained in our animal facility (Laboratory Research Center, Faculty of Medicine, University of Coimbra) and provided *ad libitum* access to food and water and maintained under controlled light (12-hour day/night cycle), temperature (22–24 °C) and humidity (50–60%). Animal handling and sacrifice followed the procedures approved by the Federation of European Laboratory Animal Science Associations (FELASA).

2.4. Cell culture, differentiation and treatment

SH-SY5Y cell line (ECACC; Sigma Aldrich) was cultured in Dulbecco's Modified Eagle's medium: nutrient mixture F-12 (DMEM-F12) supplemented with 10% fetal bovine serum (FBS), 50 U/ml penicillin and 50 μg/ml streptomycin, in humidified air with 5% CO_2 at 37 °C. In order to obtain cells with morphological and biochemical characteristics of mature neurons, SH-SY5Y cells were treated with retinoic acid (RA) (10 μM) for 1 week followed by geltrex culturing in combination with brain derived neurotrophic factor (BDNF) ((50 ng/ml), neuregulin β1 (NRG-β1–10 ng/ml) nerve growth factor (NGF-10 ng/ml), and vitamin D3 (24 nM) [21]. After complete differentiation, SH-SY5Y cells were exposed (or not – control condition) to Aβ1–42 (1–10 μM), OA (5–10 nM) and STZ (0.1–2 mM) during a period of 24 h in order to mimic AD-related alterations. Aβ1–42 was reconstituted in a 0.1% ammonia solution at the final concentration of 1 mg/ml. OA was dissolved in ethanol at the final concentration of 100 μM. A stock solution of STZ was reconstituted in DMEM- F12 medium at the concentration of 5 mg/ml. To modulate *O*-GlcNAcylation levels *in vitro*, a selective inhibitor of OGA, Thiamet-G, was used. Thiamet-G was exposed at the same time (co-treatment) and 3 h before (pre-treatment) and 3 h after (post-treatment) OA and STZ addition to the differentiated SH-SY5Y cells.

2.5. Cell viability assay-MTT tetrazolium

After the appropriate incubations, cells seeded in 24-multiwell plates were incubated with 3-(4,5-dimethylthiazol-2-yl)-2,5-diphenyltetrazolium bromide (MTT) substrate for 1 to 2 h [22]. Viable cells with active metabolism converted MTT into an insoluble purple colored formazan product, which was solubilized by acidified isopropanol. The quantity of formazan was measured by recording changes in absorbance at 570 nm using a Spectrofotometer Spectramax plus 384, being the quantity of formazan directly proportional to the number of viable cells.

2.6. Measurement of mitochondrial membrane potential

Mitochondrial membrane potential (ΔΨm) was determined using the cationic fluorescent probe tetramethylrhodamine methyl ester (TMRM+, Gibco-Invitrogen, Grand Island, NY), which accumulates predominantly in polarized mitochondria. After treatments, differentiated SH-SY5Y cells were washed with phosphate buffer saline (PBS) and incubated with sodium medium containing 300 nM TMRM+ for 1 h at 37 °C. Basal fluorescence (540 nm excitation and 590 nm emission wavelengths, with cutoff at 590 nm) was measured using a SpectraMax GEMINI EM fluorocytometer (Molecular Devices) every 30 s for a total of 3 min, followed by the addition of carbonilcyanide *p*-triflouromethoxyphenylhydrazone (FCCP; 1 μM) and oligomycin (2 μg/ml), which produced maximal mitochondrial depolarization. The difference between the increase of TMRM+ fluorescence upon addition of FCCP plus oligomycin and basal fluorescence values was used to evaluate ΔΨm. The results were expressed as percentage of control fluorescence.

2.7. Western blot analysis

Brain cortical and hippocampal samples and whole cell extracts were homogenized in ice-cold lysis buffer [20 mM Tris hydrochloride (Tris-HCl) pH 7.5, 150 mM sodium chloride (NaCl), 1 mM disodium ethylenediaminetetraacetate dehydrate (Na2EDTA), 1 mM ethylene-bis (oxyethylenenitrilo)tetraacetic acid (EGTA), 1% Triton, 2.5 mM sodium pyrophosphate, 1 mM β-glycerophosphate, 1 mM sodium orthovanadate (Na_3VO_4), 1 μg/ml leupeptin] supplemented with 0.1 M phenylmethanesulfonylfluoride (PMSF), 0.2 M dithiothreitol (DTT) and protease and phosphatases inhibitors cocktails (Roche Applied Science). The homogenates were frozen and defrozen 3 times to favor disruption, centrifuged at 14,000 rpm (Eppendorf centrifuge 5415C) for 10 min at 4 °C and the supernatant collected and stored at −80 °C. Protein concentration was determined by the bicinchoninic acid (BCA) protein assay using the BCA kit (Pierce Thermo Fisher Scientific, Rockford, IL). Equivalent amounts of protein were resolved by electrophoresis in 10% sodium dodecyl sulfate (SDS)-polyacrylamide gels and transferred to polyvinylidene fluoride (PVDF, Millipore, Billerica, MA, USA) membranes. Non-specific binding was blocked by incubation with blocking buffer [10% bovine serum albumin (BSA) in Tris-buffered saline (TBS)] for 1 h at room temperature, with gentle agitation. The blots were subsequently incubated overnight at 4 °C with gentle agitation with the specific primary antibodies. Blots were washed three times (5 min), with TBS containing 0.1% Tween (TBS-T) and then were incubated with the secondary antibodies for 1 h at room temperature with gentle agitation. After 3 washes with TBS-T (5 min), specific bands of immunoreactive proteins were visualized after membrane incubation with enhanced chemiluminescence (ECL). Images were obtained in the ChemiDoc Imaging System (Bio-Rad), and the density of protein bands calculated using the Image Lab Software (Bio-Rad).

2.8. Immuno-dot-blot assay

After PVDF membrane activation, 20 μg of human brain cortical and hippocampal homogenates, in a final volume of 5 μl, were placed in dots in specific zones of the membrane. As soon as the dots were dried, the non-specific binding reactions were blocked using 10% BSA for 1 h at room temperature. Thereafter, membranes were incubated with the respective primary antibody overnight at 4 °C with gentle agitation. Subsequently, membranes were washed 3 times with TBS-T and incubated with the secondary antibody for 1 h at room temperature. Then, after 3 washes with TBS-T, membranes were incubated with ECL and protein dots visualized using the ChemiDoc Imaging System (Bio-Rad) and the density of the protein dots quantified using the Image Lab Software (Bio-Rad).

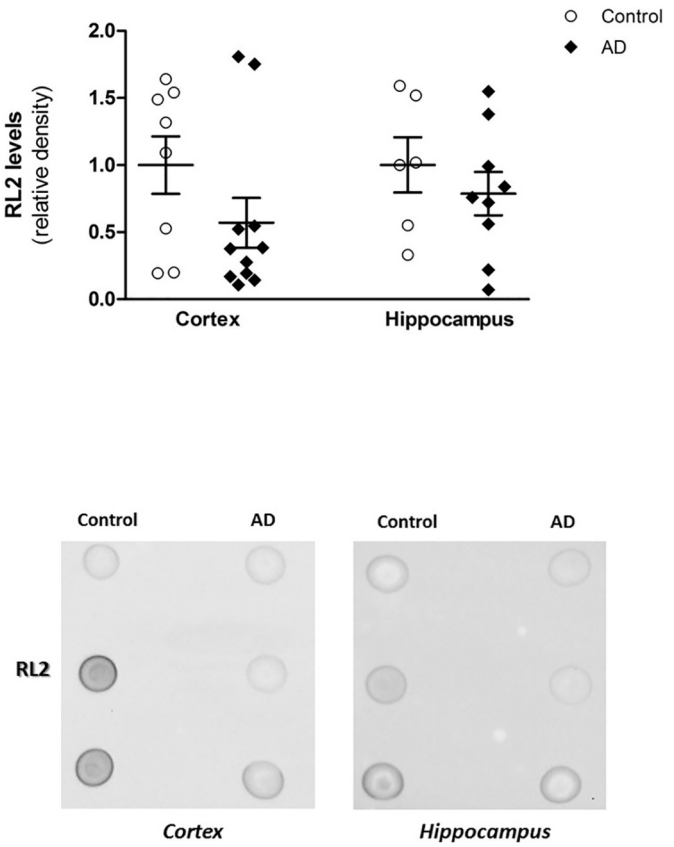

Fig. 1. *O*-GlcNAcylation levels in *post mortem* brain cortex and hippocampus of AD and control subjects. Immuno-dot-blot technique was performed using 20 μg of brain homogenates derived from AD patients and age-matched controls. Normalized *O*-GlcNAcylation levels were converted to % control. Data are expressed as mean ± SEM of 6–11 subjects' samples.

2.9. Immunocytochemistry

After the appropriate incubations, differentiated SH-SY5Y cells were fixed with 4% paraformaldehyde with sucrose 4% for 15 min at room temperature. Then, cells were permeabilized for 2 min at room temperature with 0.2% Triton-X100 in PBS and blocked for 30 min in 3% BSA. Cells were incubated for 1 h with primary antibodies prepared in 3% BSA and then washed with PBS and incubated with secondary antibodies conjugated with Alexa Fluor for 1 h at room temperature. Then, cells were washed twice with PBS and treated with Vectashield® Antifade Mounting Medium on a microscope slide. Images were acquired on a Zeiss LSM710META confocal microscope (40× 1.4NA plan-apochromat oil immersion lens).

2.10. Statistical analysis

Results are presented as mean ± standard error of the mean (SEM) of the indicated number of experiments. Statistical significance was

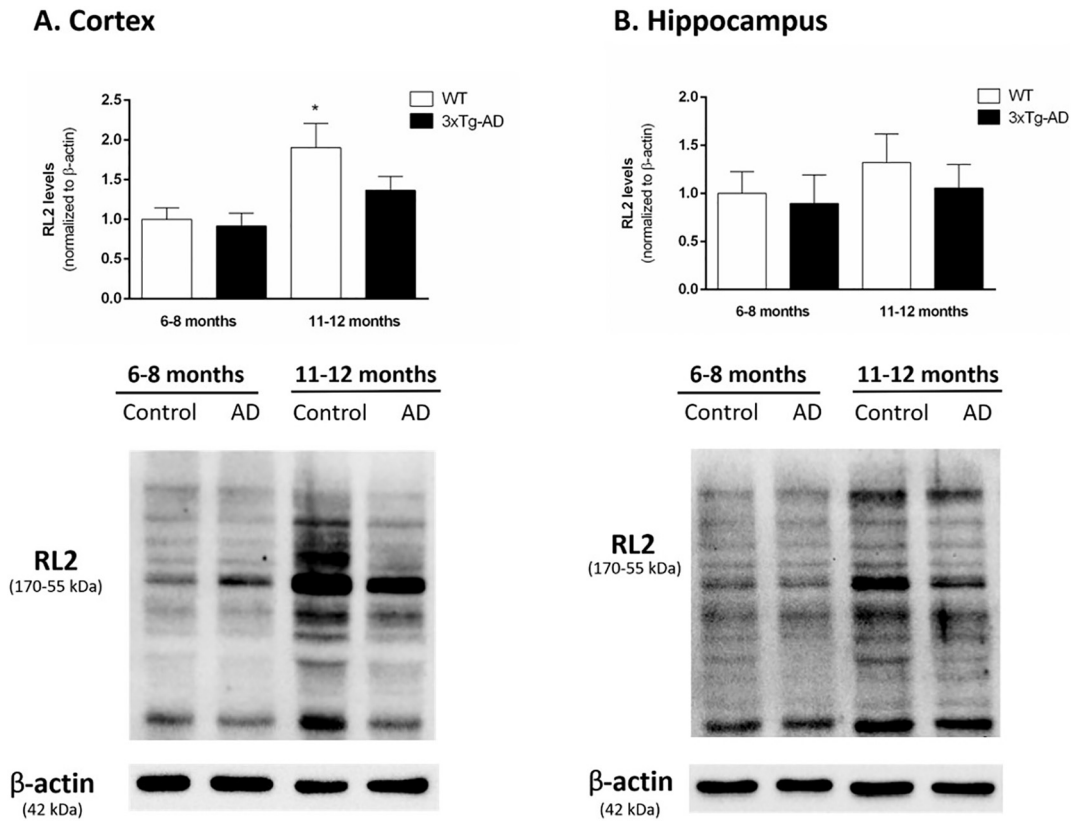

Fig. 2. *O*-GlcNAcylation levels in brain cortex (A) and hippocampus (B) of WT and 3xTg-AD mice. Brain homogenates from 6 to 8- and 11–12-month-old WT and 3xTg-AD mice were used for western blot evaluation of *O*-GlcNAcylation levels. Data are expressed as mean ± SEM of 8–9 animals from each condition studied. $^{*}p < 0.05$, when compared to the 6–8 months WT.

determined using the one-way ANOVA test for multiple comparisons, followed by the posthoc Tukey-Kramer test with the program GraphPad Prism 6 (GraphPad Software, San Diego, CA). Correlation tests were performed using Pearson's correlation analysis. Statistical significance was noted at $p < 0.05$.

3. Results

3.1. O-GlcNAc levels decrease in human AD brain

In a first approach to elucidate whether *O*-GlcNAcylation is involved in AD pathology, the global levels of this post-translational modification were evaluated in *post mortem* brain cortical and hippocampal tissue of AD and control subjects by immuno- dot-blot technique. Using the *O*-GlcNAc specific antibody RL2, a decrease in global *O*-GlcNAcylation levels was observed in AD subjects when compared with age-matched controls, this decrease being more pronounced in the brain cortex (Fig. 1).

3.2. O-GlcNAcylation levels are higher in mature mice but the levels of this posttranslational modification are lower in 3xTg-AD mice when compared to controls

In a step further, the global *O*-GlcNAcylation levels were also evaluated in brain cortical and hippocampal homogenates from 6 to 8- and 11–12-month-old WT and 3xTg-AD mice. As shown in Fig. 2A, a significant increase in *O*-GlcNAcylation levels was observed in the brain cortex of 11–12-month-old WT mice, when compared with 6–8-month-old WT mice. A similar pattern seems to occur in the hippocampus, although no statistical differences were observed (Fig. 2B). Interestingly, in the older group of animals, the levels of *O*-GlcNAcylation is lower in 3xTg-AD mice, although statistical significance is not reached.

3.3. O-GlcNAc levels reduction is strongly correlated with mitochondrial abnormalities and neuronal loss in in vitro models of AD

To gain further insights on the potential role of *O*-GlcNAcylation in AD, the global *O*-GlcNAcylation levels were evaluated in three *in vitro* models of AD and correlated with typical pathological features of the disease, such as defective mitochondrial bioenergetics and neuronal loss.

According to the amyloid cascade hypothesis, Aβ has been pinpointed as one of the major driving forces behind AD onset and progression. Aβ peptide has several isoforms, being Aβ1–42 the one predominantly found in senile plaques. Aβ1–42 is able to induce oxidative damage and neurotoxicity in differentiated SH-SY5Y neuroblastoma cells [23]. In this sense, differentiated SH-SY5Y cells were exposed to different concentrations of soluble Aβ1–42, containing monomers, oligomers and fibrils. As shown in Fig. 3C, high levels of Aβ1–42 (10 μM) promoted a drastic reduction in global *O*– GlcNAcylation levels when compared with non-treated cells. Importantly, the decrease in global *O*-GlcNAcylation levels was accompanied by the loss of cell viability (Fig. 3A) and ΔΨm (Fig. 3B). Indeed, under Aβ1–42 conditions it was observed a very strong correlation between global *O*-GlcNAcylation levels and cell viability ($r = 0.9906$) and ΔΨm ($r = 0.9264$) (Fig. 3D).

Additionally, abnormally hyperphosphorylated tau and its aggregation and deposition into NFT's also play a key role in the neuropathophysiology of AD. The dephosphorylation of tau is mostly mediated by protein phosphatases, among which serine/threonine phosphatases 1 and 2A (PP1 and PP2A) are considered to be the ones involved [24]. A previous study from our laboratory show that OA-induced PP2A inhibition promotes an increase in the levels of tau phosphorylated on Ser396 and Thr181 residues [25]. In this sense, we used OA to mimic AD-related tau pathology *in vitro*. In parallel to a significant decrease in global *O*-GlcNAcylation levels (Fig. 4B), it was

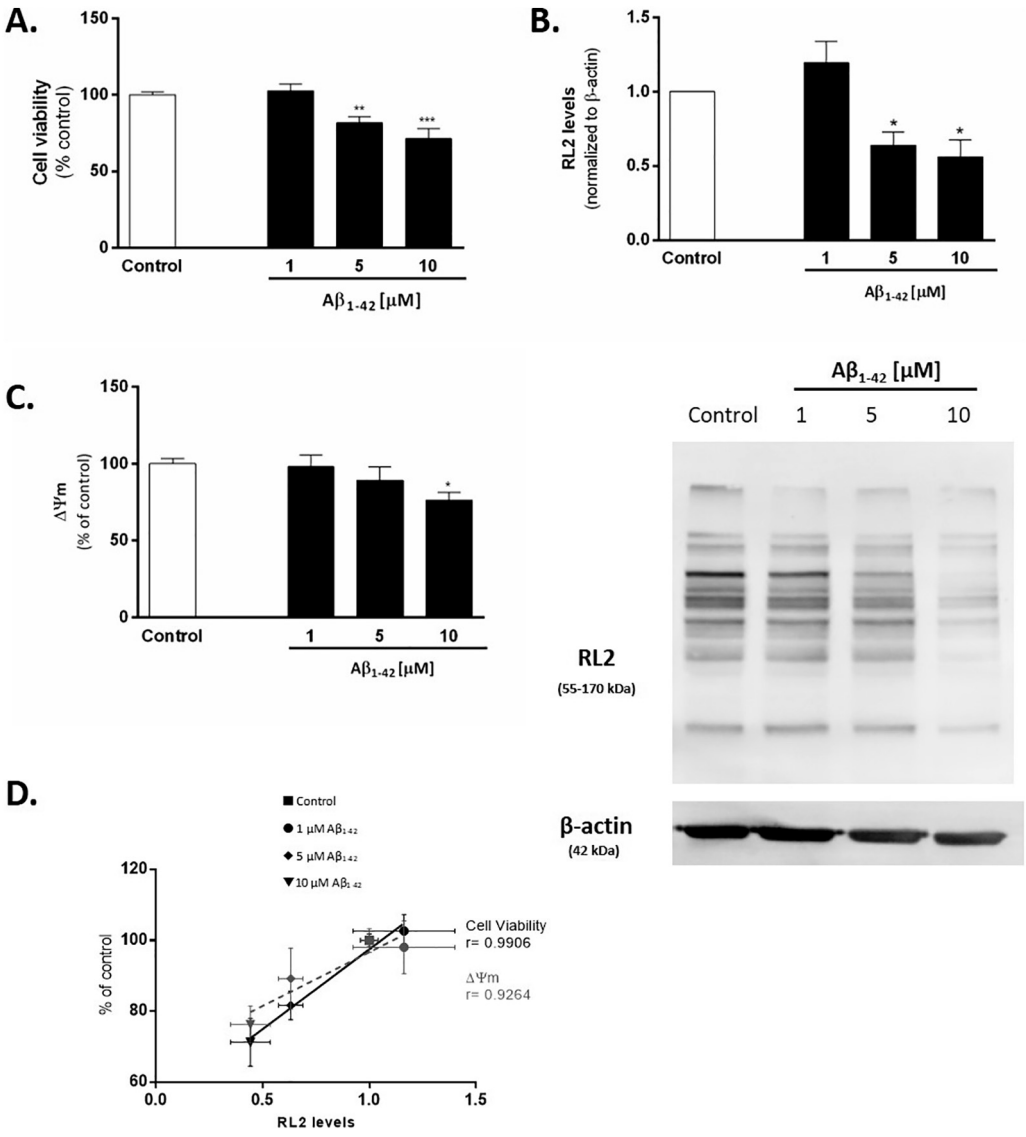

Fig. 3. Effect of Aβ1-42 on cell viability (A), *O*-GlcNAcylation levels (RL2) (B) and ΔΨm (C) and the correlation between global *O*-GlcNAcylation levels and cell viability and ΔΨm (D) in differentiated SH-SY5Y cells. Data in the graph are expressed as mean ± SEM of 4–5 independent experiments. $^{*}p < 0.05$, $^{**}p < 0.01$, $^{***}p < 0.001$ when compared to the control. $-1 < r < +1$, where $+1$ is total positive linear correlation, 0 is no linear correlation and -1 is total negative correlation.

found that the concentration of 10 nM OA induced a significant decrease in cell viability (Fig. 4A) and ΔΨm loss (Fig. 4C) when compared with non-treated cells. Again, a strong correlation between the global *O*-GlcNAcylation levels and cell viability ($r = 0.9141$) and ΔΨm ($r = 0.9879$) was observed (Fig. 4D).

Bearing in mind that most AD cases are sporadic in origin and characterized by an "insulin-resistant brain state", the intracerebroventricular administration of streptozotocin (STZ) in rodents was found to resemble several aspects of AD, including decreased brain glucose and energy metabolism [26,27], impaired brain insulin signaling [28], accumulation of tau and Aβ and learning and memory deficits. More recently, STZ was also validated *in vitro* [29,30], representing an effective *in vitro* tool to study AD. Therefore, STZ was used to reproduce *in vitro* the central insulin-resistant state that characterizes the sporadic forms of AD. Fig. 5B demonstrates that 2 mM STZ promoted a significant decrease in global *O*-GlcNAcylation levels as well as a significant reduction in cell viability (Fig. 5A) and ΔΨm (Fig. 5C). Notably, in this *in vitro* model of AD it was also found a strong correlation between the global *O*-GlcNAcylation levels and cell viability ($r = 0.9289$) and ΔΨm ($r = 0.7761$) (Fig. 5D).

Neuronal and synaptic function and integrity are in part sustained by mitochondrial network dynamics. Given the important role of post-translational modifications in regulating different aspects of mitochondrial dynamics, the next step of this study was to evaluate the effect of OA and STZ on mitochondrial morphology and distribution. Confocal microscopy analysis revealed that non-treated cells contain mostly tubular mitochondria, distributed evenly throughout the whole cell (Fig. 6). However, the exposure of differentiated SH-SY5Y cells to OA (10 nM) and STZ (2 mM) triggered the collapse of mitochondrial network (Fig. 6). Regarding STZ, a slight reduction in the number of individual mitochondria and mitochondrial networks per nucleus/neuronal cell, number of branches and mitochondrial footprint was observed. Conversely, a significant increase of the average length of all rods/branches was observed (Figs. 6 and 7). OA, in turn, induced a massive accumulation of smaller and rounder mitochondria in the perinuclear region, with a significant decrease in the number of individual mitochondria and mitochondria networks per nucleus/neuronal cells as well as mitochondrial footprint (Figs. 6 and 7). Overall, these observations suggest that the neurotoxic agents disrupt microtubule network leading to a neuritic retraction.

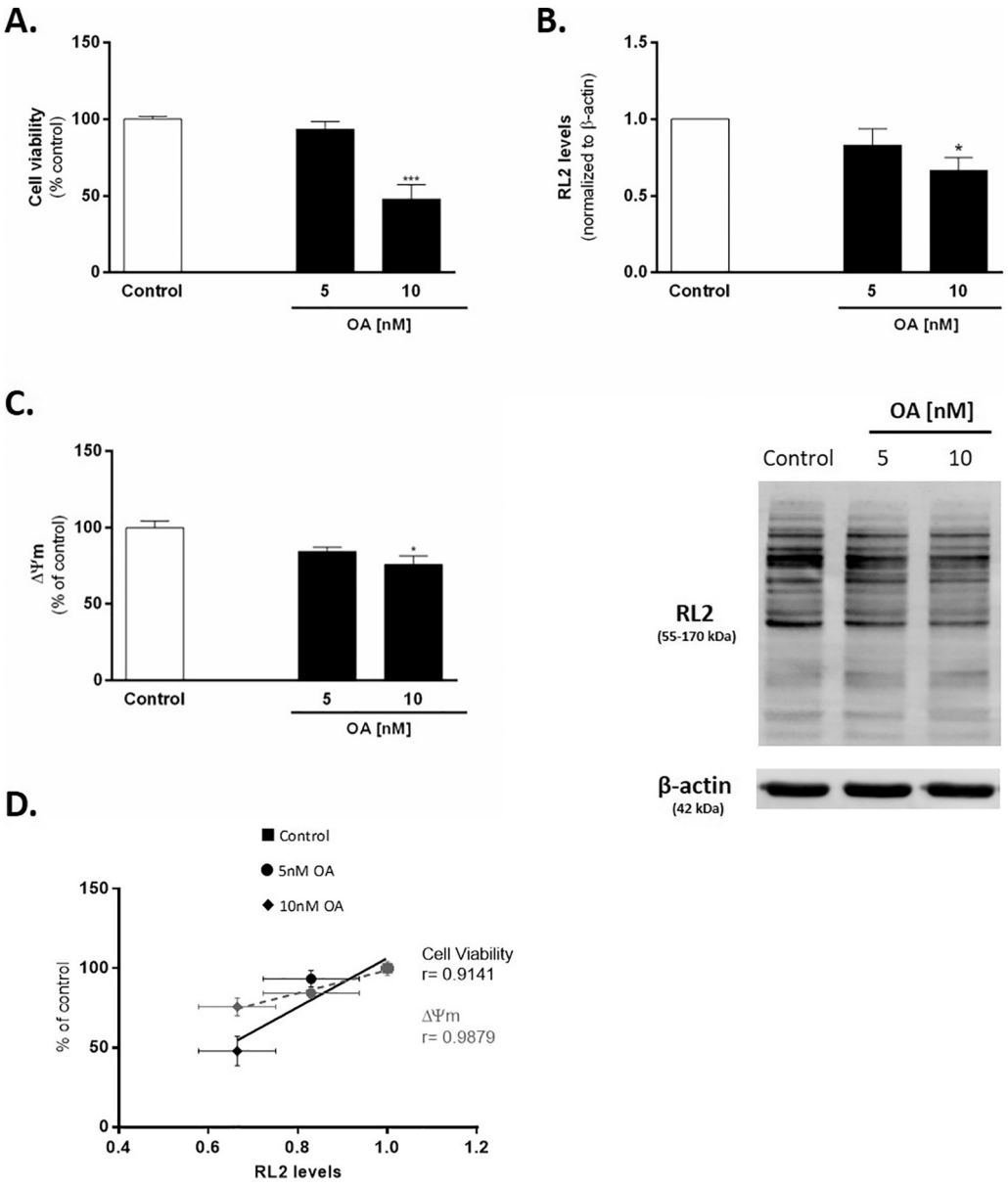

Fig. 4. Effect of OA on cell viability (A), *O*-GlcNAcylation levels (RL2) (B) and ΔΨm (C) and the correlation between global *O*-GlcNAc levels and cell viability and ΔΨm (D) in differentiated SH-SY5Y cells. Data in the graph are expressed as mean ± SEM of 4–5 independent experiments. $*p < 0.05$, $**p < 0.01$, $***p < 0.001$ when compared to the control. $-1 < r < +1$, where +1 is total positive linear correlation, 0 is no linear correlation and −1 is total negative correlation.

3.4. Thiamet-G increases O-GlcNAcylation levels without affecting cell viability and mitochondrial bioenergetic function

With the purpose of modulating *O*-GlcNAcylation *in vitro* to evaluate the potential therapeutic role of this post-translational modification, Thiamet-G was used as a pharmacological strategy to increase *O*-GlcNAcylation levels through the inhibition of OGA. Based on the available literature, differentiated SH-SY5Y cells were exposed to a range of Thiamet-G concentrations from 0.025 to 3 μM. As shown in Fig. 8, 3 μM of Thiamet-G induced the most robust increase in global *O*-GlcNAcylation levels at 3 h that persists until 24 h of incubation. Of note, all the concentrations of Thiamet-G tested did not significantly affect cell viability (Fig. 8A) and ΔΨm (Fig. 8B). Overall, this data indicates that Thiamet-G *per se* is able to modulate *O*-GlcNAcylation without a negative impact on neuronal cells homeostasis.

3.5. Thiamet-G averts loss of O-GlcNAcylation and cell viability in in vitro models of AD

In the last set of experiments the potential protective effect of Thiamet-G against the AD-related pathological events was investigated in our *in vitro* models of the disease. Three different strategies were applied to evaluate the therapeutic potential of Thiamet- G: pre-, co- and post-treatment. As shown in Fig. 9, pre-, co- and post-treatment with 3 μM Thiamet-G were able to counteract the reduction in global *O*-GlcNAc levels triggered by OA (10 nM) and STZ (2 mM). However, only the pre-treatment with Thiamet-G was able to prevent the loss of cell viability in these *in vitro* models of AD (Fig. 10).

4. Discussion

The present study shows reduced levels of *O*-GlcNAcylation in several models of AD. Notably, a strong correlation was established between global *O*-GlcNAcylation levels and some AD-associated

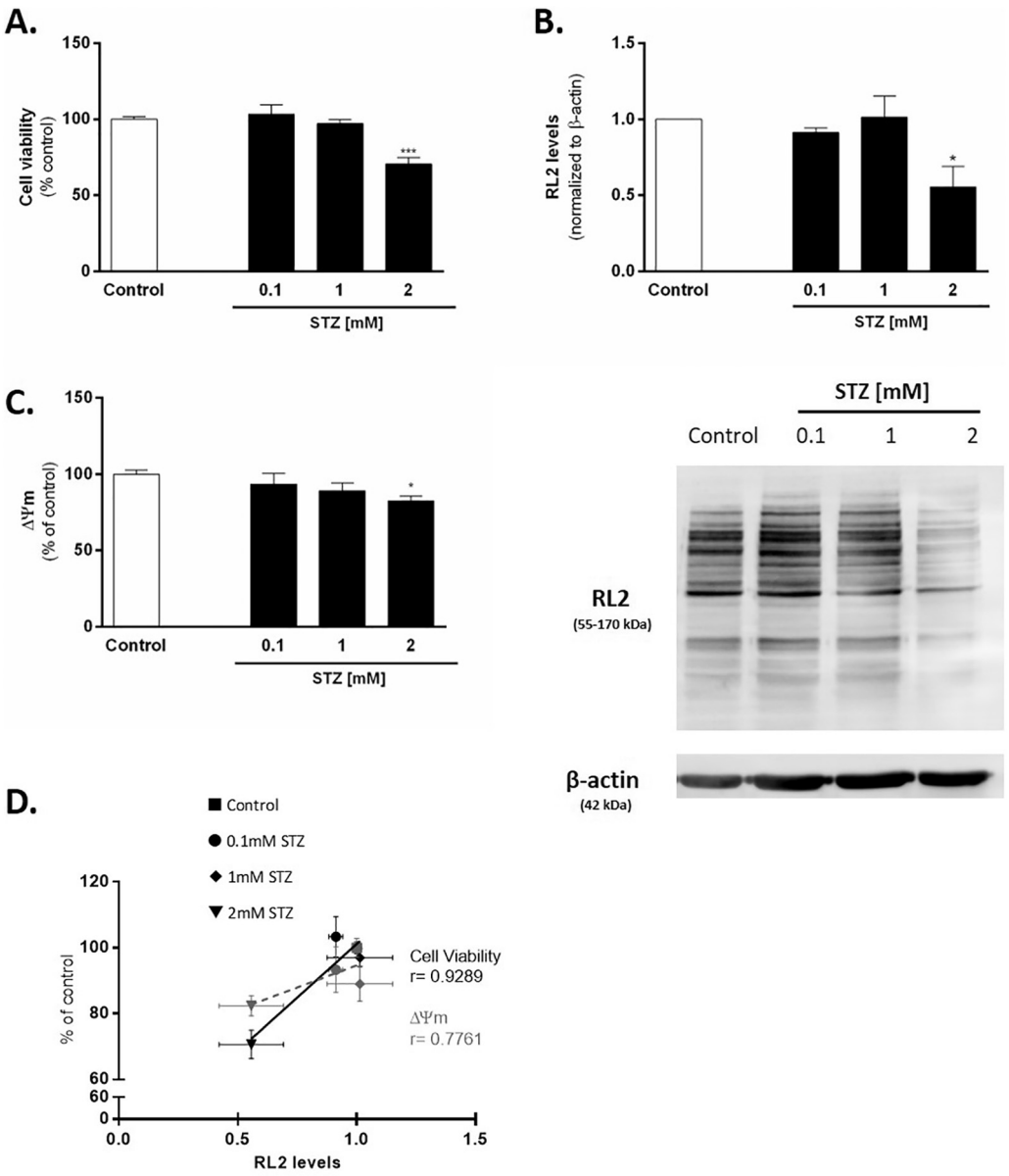

Fig. 5. Effect of STZ on cell viability (A), *O*-GlcNAcylation levels (RL2) (B) and ΔΨm (C) and the correlation between global *O*-GlcNAc levels and cell viability and ΔΨm (D) in differentiated SH-SY5Y cells. Data in the graph are expressed as mean ± SEM of 4–5 independent experiments. $^{*}p < 0.05$, $^{**}p < 0.01$, $^{***}p < 0.001$ when compared to the control. $-1 < r < +1$, where $+1$ is total positive linear correlation, 0 is no linear correlation and -1 is total negative correlation.

pathological features, including hampered mitochondrial bioenergetic function and altered mitochondrial morphology and distribution. Importantly, the pharmacological increase in *O*-GlcNAcylation levels by Thiamet-G, which inhibits OGA, averted the loss of *O*-GlcNAcylation levels and cell viability in *in vitro* models of the disease, reinforcing the idea that targeting this posttranslational modification may constitute a feasible therapeutic intervention to tackle AD pathology.

Faulty cerebral glucose metabolism has been pinpointed as a contributing factor underlying the neurodegenerative events that occur in AD [31]. PET studies using 2-fluoro-2-deoxy-glucopyranose (FDG) showed a progressive decline in cerebral glucose metabolism in AD [32,33]. Of note, lessons from clinical and experimental studies revealed that the decline in brain glucose uptake and metabolism occurs decades before the onset of AD symptoms and histopathological changes suggesting that metabolic deficits occur early in the course of AD [34]. Using post-mortem human brain tissue, we observed a reduction of global *O*-GlcNAcylation levels in brain tissue from AD subjects, this reduction being more pronounced in brain cortex (Fig. 1), which is in accordance with the observations made by Liu and collaborators [35]. As a plausible explanation, these authors attributed the reduction in *O*-GlcNAcylation to reduced neuronal glucose availability due to down-regulation of glucose transporters (GLUT) 1 and GLUT3 in the AD brain [36]. A recent study shows that the activation of calpain 1 causes GLUT3 proteolysis and downregulation of *O*-GlcNAcylation in AD brains [34]. In contrast, Förster and collaborators detected augmented cytosolic *O*-GlcNAc levels in brain tissue from AD subjects [37]. Those conflicting observations may be the result of the analyses of different *post mortem* brain tissue regions at different stages of the disease conjugated with different analysis methods as well as the use of different anti-*O*-GlcNAc antibodies. Furthermore, *O*-GlcNAcylation levels fluctuate depending on the *post mortem* interval [38] and stage of the disease.

Additionally, we observed an increase in global *O*-GlcNAcylation levels in brain tissue from mature mice, an effect more pronounced in brain cortex from WT mice (Fig. 2). In fact, it is known that age alters brain glucose metabolism [39] modulating *O*-GlcNAcylation levels. In

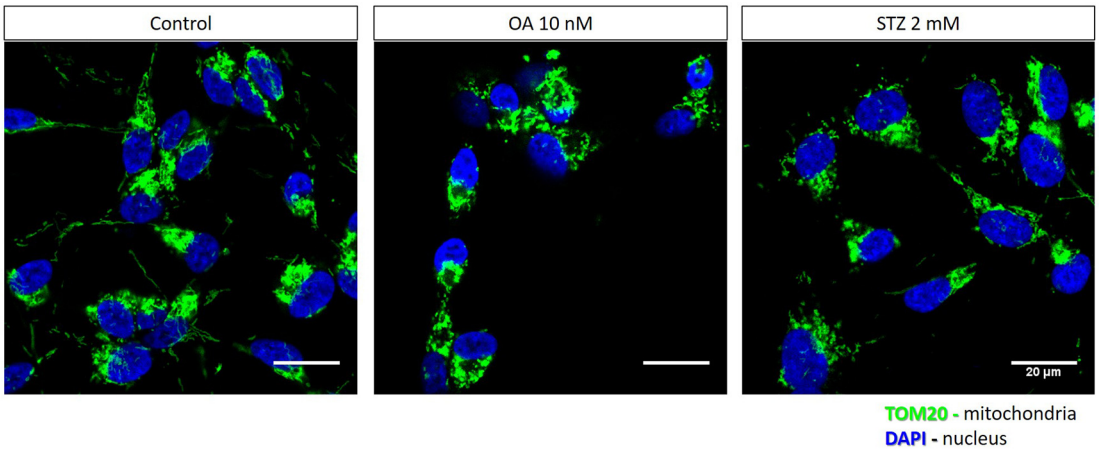

Fig. 6. Effect of OA and STZ on neuronal morphology and mitochondrial network in differentiated SH-SY5Y cells. OA and STZ were applied to differentiated SH-SY5Y cells during a period of 24 h, fixed and mitochondria marked with TOM20 antibody (green), and nuclei with DAPI (blue) and visualized by confocal microscopy at 63× magnification. Images are representative of 3 independent experiments.

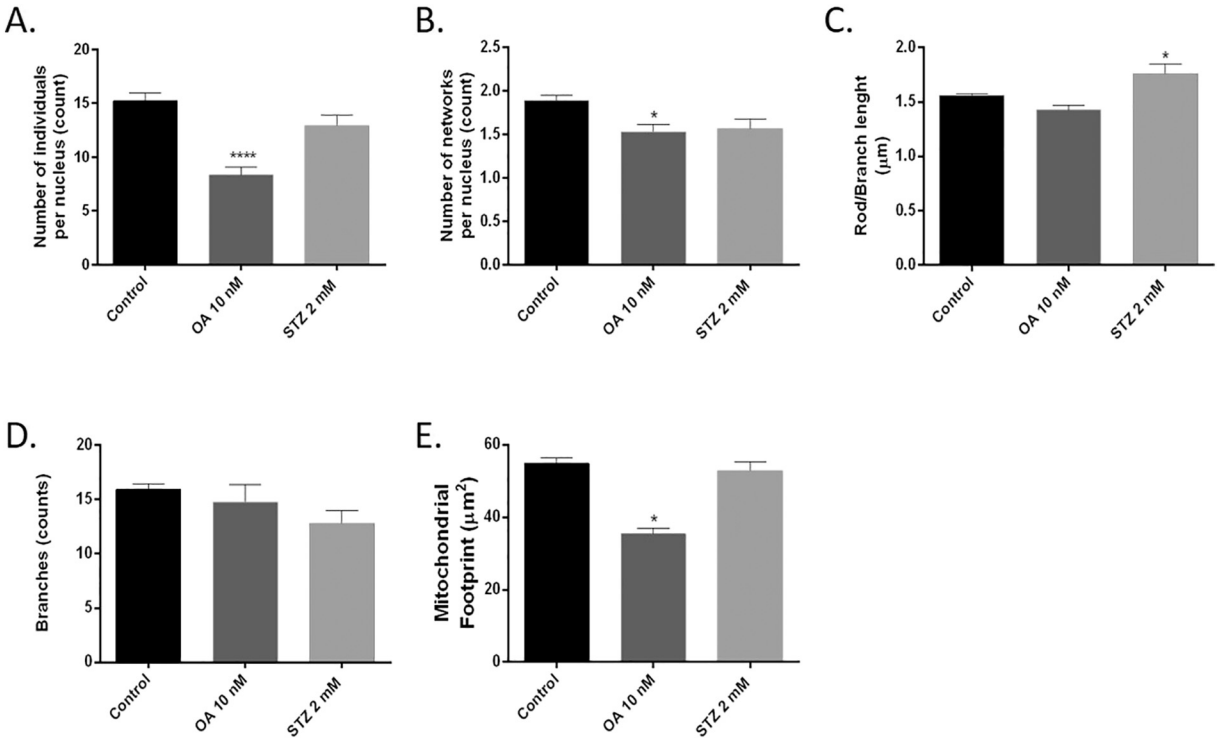

Fig. 7. Results from mitochondrial network analysis using the Mitochondrial Network Analysis (MiNA) toolset from ImageJ on differentiated SH-SY5Y cells: number of individuals per nucleus (A), number of networks per nucleus (B), the average length of all rods/branches (C), mean branches per network (D) and mitochondrial footprint (E). Data in the graph are expressed as mean ± SEM of 3 independent experiments. $*p < 0.05$, $**p < 0.01$, $***p < 0.001$ when compared to the control.

accordance with our observations, Fülöp et al. [40] observed an increase in the levels of this posttranslational modification in the brain of aged Brown-Norway rats. However, other studies revealed a decrease in *O*-GlcNAcylation levels in aged mice [41,42] rendering the brain more prone to dysfunction under stress conditions such as brain ischemia. However, those studies used 22–24-month-old WT mice while in our study we used younger (11–12-month old) mice. In our study, 11–12-month-old 3xTg-AD mice show a reduction in brain *O*-GlcNAcylation levels, an effect more pronounced in brain cortex (Fig. 2). Accordingly, a recent study performed in 12-month-old 3xTg-AD mice shows a decrease of total *O*-GlcNAcylation levels associated with altered OGT and OGA activation [43]. Proteomics analysis identified several proteins with reduced *O*-GlcNAcylation levels, which belong to key pathways involved in the AD progression such as neuronal structure, protein degradation and glucose metabolism [43]. In accordance the proteomic quantitative analysis performed by Wang and colleagues [44] revealed that *post mortem* AD brain tissue presents altered *O*-GlcNAcylated proteins belonging to several structural and functional categories such as synaptic, cytoskeleton and memory-associated proteins. Besides that, altered *O*-GlcNAcylation cycling might result in abnormal *O*-GlcNAcylated tau and APP contributing to the accumulation of toxic species in the brain supporting the idea that impaired *O*-GlcNAcylation levels contribute to the progression of AD [34].

The exposure of differentiated SH-SY5Y cells to Aβ1–42 (Fig. 3C), OA (Fig. 4C) or STZ (Fig. 5C) induced a significant decrease in global *O*-GlcNAcylation levels. Evidence from the literature supports our observations since both Aβ and tau can be modified by *O*-GlcNAcylation [34]. It was shown that the increase in *O*-GlcNAcylated APP,

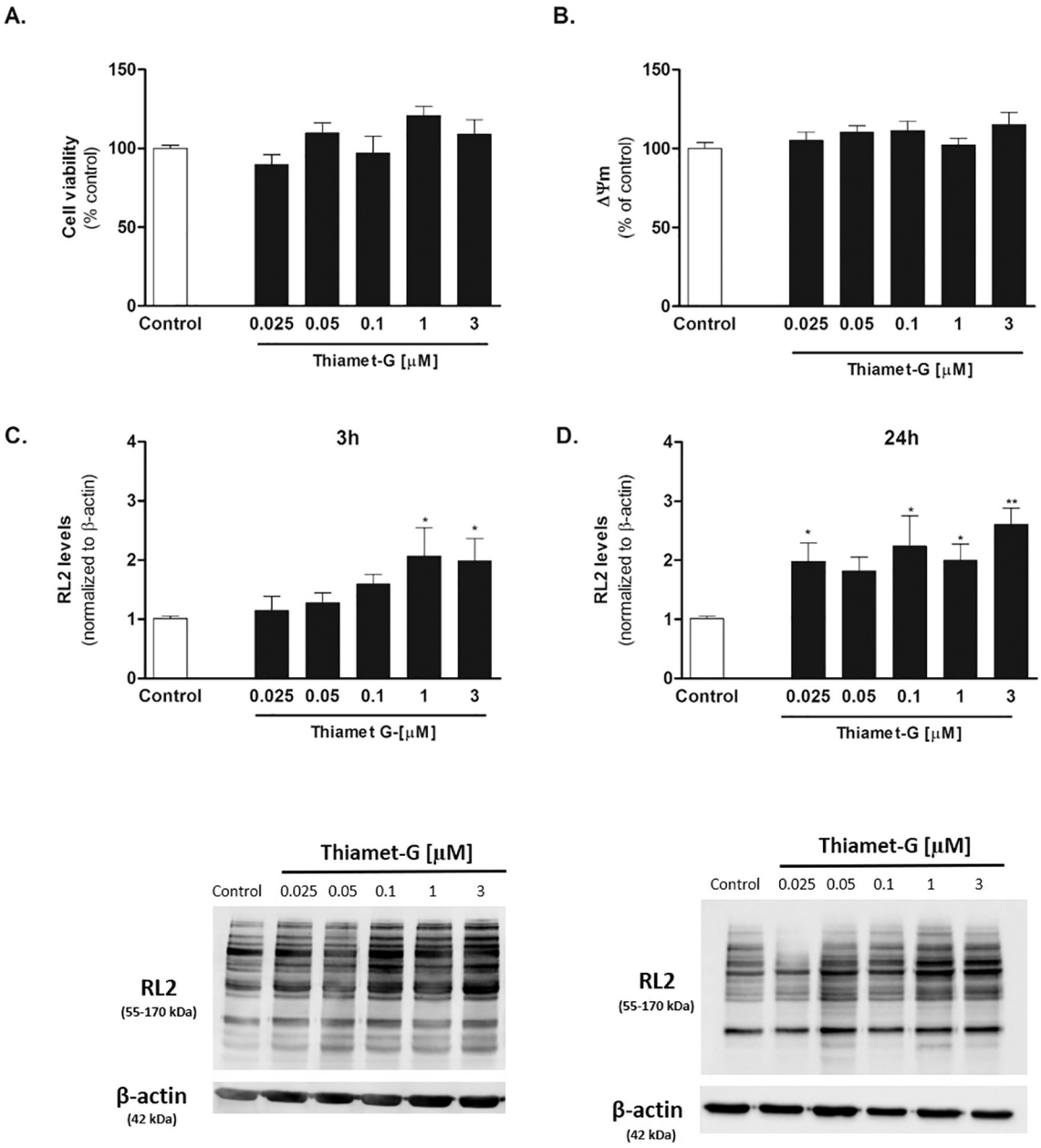

Fig. 8. Effect of Thiamet-G on cell viability (A), ΔΨm (B) and *O*-GlcNAcylation levels (C–D) in differentiated SH-SY5Y cells. For cell viability and ΔΨm experiments, cells were exposed to different concentrations of Thiamet-G for 24 h. For evaluation of *O*-GlcNAc levels with RL2 antibody, cells were exposed to different concentrations of Thiamet-G for periods of 3 and 24 h. Data in the graph are expressed as mean ± SEM of 6 independent experiments. $^{*}p < 0.05$, $^{**}p < 0.01$ when compared to the control.

particularly at threonine 576 residue [45], promotes its trafficking rate to the plasma membrane and decreases its endocytosis rate, resulting in decreased Aβ production [45–47]. It was also reported that genetic and pharmacological tools that increase the levels of *O*-GlcNAcylation increase non-amyloidogenic α-secretase processing resulting in increased levels of the neuroprotective sAPPα fragment and decreased Aβ secretion [48]. A reciprocal relationship between *O*-GlcNAcylation levels and phosphorylation was also documented during the pathological course of AD. Using starved mice to mimic AD-related hypometabolism Liu and collaborators [38] reported that decreased *O*-GlcNAcylation levels are associated with increased tau hyperphosphorylation. Interestingly, hyperphosphorylated tau contains 4-fold less *O*-GlcNAcylation than non-hyperphosphorylated tau, which fosters the relationship between *O*-GlcNAcylation and phosphorylation of tau in the human brain [35].

The present study also establishes a strong correlation between global *O*-GlcNAcylation levels and cellular viability and ΔΨm (Figs. 3D, 4D, 5D) in three different *in vitro* models of AD. The loss of cell viability that accompanies *O*-GlcNAcylation reduction in these *in vitro* models of AD is not surprising taking into account that this posttranslational modification is particularly enriched in neuronal synapses [19,49] and modifies several post-synaptic density proteins [50]. Regarding ΔΨm decay, it was recently found that mitochondrial components are modified by *O*-GlcNAcylation. An elegant study from Cha and collaborators revealed that ATP synthase subunit α (ATP5A) is a substrate of *O*-GlcNAcylation [51]. Remarkably, these authors observed that *O*-GlcNAcylation of ATP5A is decreased in AD pathology since Aβ blocks the direct interaction between ATP5A and mitochondrial OGT leading to impaired ATPase activity and ATP depletion [51]. Another study showed that disruption of posttranslational modification of proteins

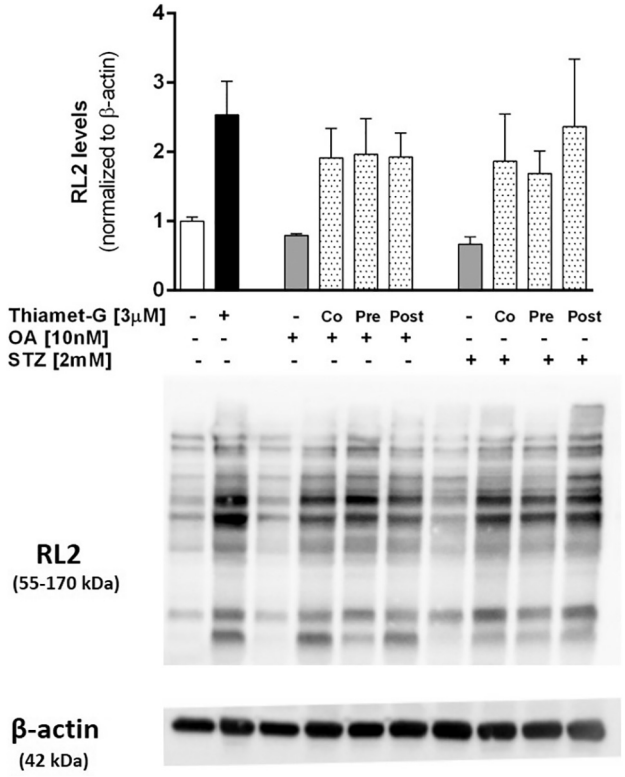

Fig. 9. Effect Thiamet-G on *O*-GlcNAc levels in OA- and STZ-induced *in vitro* models of AD. Thiamet-G was exposed at the same time (co-treatment) or 3 h before (pre-treatment) or after (post-treatment) OA and STZ addition to the differentiated SH-SY5Y cells. Data in the graph are expressed as mean ± SEM of 3 independent experiments. $*p < 0.05$, $**p < 0.01$ when compared to the control.

with *O*-GlcNAcylation *via* overexpression of OGT or OGA impairs mitochondrial function [52]. More recently, it was reported that sustained *O*-GlcNAcylation elevation in SH-SY5Y neuroblastoma cells increase OGA expression and reduced cellular respiration and ROS generation and cells with elevated *O*-GlcNAcylation levels had elongated mitochondria and increased ΔΨm [53]. The same study shows that OGT knockdown in the liver of mice increases ROS levels and the nuclear respiratory factor (NRF) 2 antioxidant response and impairs respiration [53]. Using siRNA in HeLa cells, Sacoman and colleagues [54] found that reducing endogenous mitochondrial OGT (mOGT) expression leads to alterations in mitochondrial structure and function, including dynamin-related protein (Drp)1-dependent mitochondrial fragmentation, reduction in ΔΨm, and a significant loss of mitochondrial content in the absence of mitochondrial ROS. We also evaluated the impact of reduced *O*-GlcNAcylation on mitochondrial morphology and distribution in *in vitro* models of AD. In our study the exposure of differentiated SH-SY5Y to OA and STZ promoted the collapse of mitochondrial network as evidenced by the perinuclear accumulation of smaller and rounder mitochondria, these alterations being more pronounced in the OA-induced model of AD (Fig. 6). It has been reported that the mitochondrial motor-adaptor Milton that tethers mitochondria to the kinesin motors facilitating the anterograde movement of mitochondria is targeted by *O*-GlcNAcylation, being a substrate for OGT. Briefly, during synaptic activity Milton's *O*-GlcNAcylation arrests the motile pool of mitochondria in pre- and post-synaptic areas in order to assure ATP production and Ca^{2+} buffering essential for synapse maintenance, acting as a stop signal [20]. In this sense, it is tempting to speculate that loss of Milton *O*-GlcNAcylation underlies mitochondrial mislocalization in AD, leading to a drastic reduction in the stationary mitochondrial pool at the synapses, which in turn contributes to an energetic catastrophe that culminates in synaptic "starvation" and neuronal loss. However, several components of the mitochondrial fusion-fission and trafficking machinery should be evaluated in future experiments to gain further insights on the relation between *O*-GlcNAcylation and mitochondrial dynamics in AD pathology.

At this point, it is at least clearly known that *O*-GlcNAcylation plays a significant role in AD pathophysiology which makes this post-translational modification an attractive target to tackle this devastating neurodegenerative disease. Using a pharmacological approach to modulate *O*-GlcNAcylation in differentiated SH-SY5Y cells, this study reveals that Thiamet-G is able to induce a robust augment in global *O*-GlcNAcylation levels (Fig. 8C and D) without affecting neither cell viability (Fig. 8A) nor ΔΨm (Fig. 8B). Accordingly, Yuzwa and collaborators demonstrated that Thiamet-G increases *O*-GlcNAcylation levels in PC12 cells and no signs of toxicity were detected [55]. Concerning the protective potential of Thiamet-G, we found that only the pre-treatment with Thiamet- G was able to prevent loss of *O*-GlcNAcylation levels (Fig. 9) and cell viability (Fig. 10) demonstrating that under our *in vitro* experimental settings Thiamet-G demonstrated a preventive role. It has been previously demonstrated that Thiamet-G increases *O*-GlcNAcylation levels in JNPL3 transgenic mice, which express a mutant hyperphosphorylated and aggregate-prone tau isoform, and decreases the extent of NFTs in the brain, slowing down tau-driven neurodegeneration [56]. The same authors also found that increased *O*-GlcNAcylation decreases the formation of tau aggregates *in vitro*, without changing its structural monomeric form, causing neuronal cell loss [56,57]. In the same line, Hastings and colleagues [58] reported that chronic inhibition of OGA, through genetic and pharmacological approaches, reduces pathological tau in the brain and total tau in cerebrospinal fluid of rTg4510 mice probably by directly increasing *O*-GlcNAcylation of tau and thereby maintaining tau in the soluble, non-

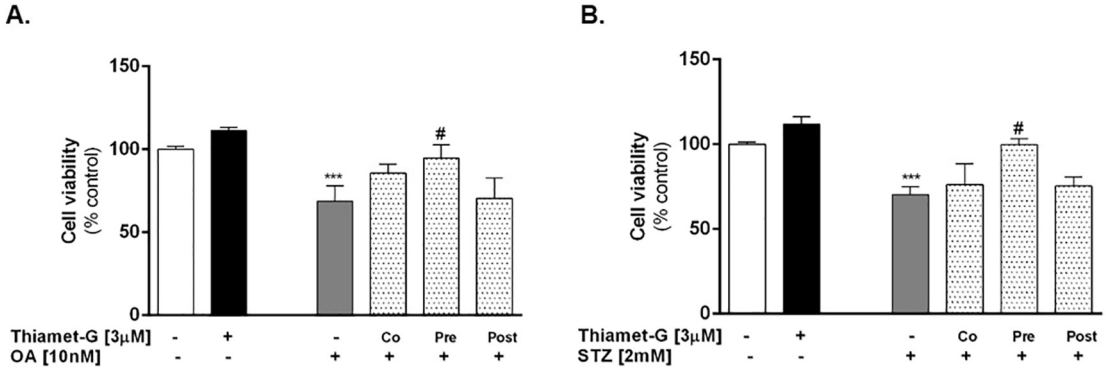

Fig. 10. Effect Thiamet-G on cell viability in OA- (A) and STZ-induced (B) *in vitro* models of AD. Thiamet-G was exposed at the same time (co-treatment) or 3 h before (pre-treatment) or after (post-treatment) OA and STZ addition to the differentiated SH-SY5Y cells. Data in the graph are expressed as mean ± SEM of 5 independent experiments. $*p < 0.05$, $**p < 0.01$, $***p < 0.001$ when compared to the control. $\#p < 0.05$ when compared to OA or STZ alone.

toxic form by reducing tau aggregation. Yuzwa and colleagues also demonstrated that Thiamet-G increases *O*-GlcNAcylation, attenuates Aβ burden, the formation of neuritic plaques and memory deficits in a mice bearing both mutated human tau and APP (TAPP mice) [59]. Another OGA inhibitor, 1,2-dideoxy-2′-propyl-α-D-glucopyranoso-[2,1-D]-Δ2′-thiazoline (NButGT), caused a reduction of Aβ production by lowering γ-secretase activity both *in vitro* and *in vivo* [60]. Moreover, NButGT attenuated the accumulation of Aβ, neuroinflammation, and memory impairment in the 5XFAD mice [60].

5. Conclusion

Our results support the idea that reduced *O*-GlcNAcylation underlies AD pathology representing a “sweet” route to tackle this devastating neurodegenerative disease. However, further studies are required to clarify the key mechanisms associated to the loss O-GlcNAcylation that contribute to the onset and/or aggravation of AD pathology.

Transparency document

The Transparency document associated with this article can be found, in online version.

Acknowledgements

Sónia C. Correia has a post-doctoral fellowship (SFRH/BPD/109822/2015) from the Fundação para a Ciência e a Tecnologia (FCT). Tiffany S. Pinho is recipient of a research fellowship from the Healthy Aging 2020 (CENTRO-01-0145-FEDER-000012). The authors' work is supported by FEDER funds through the Operational Programme Competitiveness Factors — COMPETE, national funds by FCT under the project PEst-C/SAU/LA0001/2013-2014 and strategic project UID/NEU/04539/2013 and Santa Casa da Misericórdia de Lisboa - Mantero Belard Award 2015 (MB-1049-2015).

References

[1] L.A. Demetrius, J. Driver, Alzheimer's as a metabolic disease, Biogerontology 14 (2013) 641–649.
[2] J. Hroudová, N. Singh, Z. Fišar, Mitochondrial dysfunctions in neurodegenerative diseases: relevance to Alzheimer's disease, Biomed. Res. Int. 2014 (175062) (2014).
[3] S.C. Correia, et al., Mitochondrial abnormalities in a streptozotocin-induced rat model of sporadic Alzheimer's disease, Curr. Alzheimer Res. 10 (2013) 406–419.
[4] H. Braak, R.A. de Vos, E.N. Jansen, H. Bratzke, E. Braak, Neuropathological hallmarks of Alzheimer's and Parkinson's diseases, Prog. Brain Res. 117 (1998) 267–285.
[5] J.K. Morris, R. a Honea, E.D. Vidoni, R.H. Swerdlow, J.M. Burns, Is Alzheimer's disease a systemic disease? Biochim. Biophys. Acta 1842 (2014) 1340–1349.
[6] H. Braak, E. Braak, Staging of Alzheimer's disease-related neurofibrillary changes, Neurobiol. Aging 16 (1995) 278–284.
[7] S.C. Correia, et al., Insulin signaling, glucose metabolism and mitochondria: major players in Alzheimer's disease and diabetes interrelation, Brain Res. 1441 (2012) 64–78.
[8] Z. Chen, C. Zhong, Decoding Alzheimer's disease from perturbed cerebral glucose metabolism: implications for diagnostic and therapeutic strategies, Prog. Neurobiol. 108 (2013) 21–43.
[9] J.L. Chou, et al., Early dysregulation of the mitochondrial proteome in a mouse model of Alzheimer's disease, J. Proteome 74 (2011) 466–479.
[10] A. Nunomura, et al., Oxidative damage is the earliest event in Alzheimer disease, J. Neuropathol. Exp. Neurol. 60 (2001) 759–767.
[11] R. Resende, et al., Brain oxidative stress in a triple-transgenic mouse model of Alzheimer disease, Free Radic. Biol. Med. 44 (2008) 2051–2057.
[12] J. Yao, et al., Mitochondrial bioenergetic deficit precedes Alzheimer's pathology in female mouse model of Alzheimer's disease, Proc. Natl. Acad. Sci. 106 (2009) 14670–14675.
[13] R.P. Friedland, et al., Regional cerebral glucose transport and utilization in Alzheimer's disease, Neurology 39 (1989) 1427–1434.
[14] W.J. Jagust, et al., Diminished glucose transport in Alzheimer's disease: dynamic PET studies, J. Cereb. Blood Flow Metab. 11 (1991) 323–330.
[15] J.C. Trinidad, et al., Global identification and characterization of both O-GlcNAcylation and phosphorylation at the murine synapse, Mol. Cell. Proteomics 11 (2012) 215–229.
[16] C.R. Torres, G.W. Hart, Topography and polypeptide distribution of terminal N-acetylglucosamine residues on the surfaces of intact lymphocytes. Evidence for O-linked GlcNAc, J. Biol. Chem. 259 (1984) 3308–3317.
[17] C. Butkinaree, K. Park, G.W. Hart, O-linked beta-N-acetylglucosamine (O-GlcNAc): extensive crosstalk with phosphorylation to regulate signaling and transcription in response to nutrients and stress, Biochim. Biophys. Acta 1800 (2010) 96–106.
[18] A.C. Wang, E.H. Jensen, J.E. Rexach, H.V. Vinters, L.C. Hsieh-Wilson, Loss of O-GlcNAc glycosylation in forebrain excitatory neurons induces neurodegeneration, Proc. Natl. Acad. Sci. 113 (2016) 15120–15125.
[19] R.N. Cole, G.W. Hart, Cytosolic O-glycosylation is abundant in nerve terminals, J. Neurochem. 79 (2001) 1080–1089.
[20] G. Pekkurnaz, J. Trinidad, X. Wang, D. Kong, T. Schwarz, Glucose regulates mitochondrial motility via Milton modification by O-GlcNAc transferase, Cell 158 (2014) 54–68.
[21] L. Agholme, T. Lindström, K. Kågedal, J. Marcusson, M. Hallbeck, An in vitro model for neuroscience: differentiation of SH-SY5Y cells into cells with morphological and biochemical characteristics of mature neurons, J. Alzheimers Dis. 20 (2010) 1069–1082.
[22] T.L. Riss, et al., Cell Viability Assays. Assay Guidance Manual, Eli Lilly & Company and the National Center for Advancing Translational Sciences, 2004.
[23] J. Krishtal, O. Bragina, K. Metsla, P. Palumaa, V. T?Ugu, Toxicity of amyloid beta 1-40 and 1-42 on SH-SY5Y cell line, Springerplus 4 (2015) P19.
[24] F. Liu, I. Grundke-Iqbal, K. Iqbal, C.-X. Gong, Contributions of protein phosphatases PP1, PP2A, PP2B and PP5 to the regulation of tau phosphorylation, Eur. J. Neurosci. 22 (2005) 1942–1950.
[25] A.I. Plácido, et al., Phosphatase 2A inhibition affects endoplasmic reticulum and mitochondria homeostasis via cytoskeletal alterations in brain endothelial cells, Mol. Neurobiol. 54 (2017) 154–168.
[26] H. Siebner, et al., Cerebral metabolic changes accompanying conversion of mild cognitive impairment into Alzheimer's disease: a PET follow-up study, Eur. J. Nucl. Med. Mol. Imaging 30 (2003) 1104–1113.
[27] W.D. Heiss, B. Szelies, J. Kessler, K. Herholz, Abnormalities of energy metabolism in Alzheimer's disease studied with PET, Ann. N. Y. Acad. Sci. 640 (1991) 65–71.
[28] Y. Liu, F. Liu, I. Grundke-Iqbal, K. Iqbal, C.-X. Gong, Deficient brain insulin signalling pathway in Alzheimer's disease and diabetes, J. Pathol. 225 (2011) 54–62.
[29] K. Plaschke, J. Kopitz, In vitro streptozotocin model for modeling Alzheimer-like changes: effect on amyloid precursor protein secretases and glycogen synthase kinase-3, J. Neural Transm. 122 (2015) 551–557.
[30] J. Biswas, et al., Streptozotocin induced neurotoxicity involves Alzheimer's related pathological markers: a study on N2A cells, Mol. Neurobiol. 53 (2016) 2794–2806.
[31] L. Mosconi, Glucose metabolism in normal aging and Alzheimer's disease: methodological and physiological considerations for PET studies, Clin. Transl. Imaging 1 (2013).
[32] V. Calsolaro, P. Edison, Alterations in glucose metabolism in Alzheimer's disease, Recent Pat. Endocr. Metab. Immune Drug Discov. 10 (2016) 31–39.
[33] L. Mosconi, et al., FDG-PET changes in brain glucose metabolism from normal cognition to pathologically verified Alzheimer?S disease, Eur. J. Nucl. Med. Mol. Imaging 36 (2009) 811–822.
[34] T.S. Pinho, D.M. Verde, S.C. Correia, S.M. Cardoso, P.I. Moreira, O-GlcNAcylation and neuronal energy status: implications for Alzheimer's disease, Ageing Res. Rev. 46 (2018) 32–41.
[35] F. Liu, et al., Reduced O-GlcNAcylation links lower brain glucose metabolism and tau pathology in Alzheimer's disease, Brain 132 (2009) 1820–1832.
[36] Y. Liu, F. Liu, K. Iqbal, I. Grundke-Iqbal, C.-X. Gong, Decreased glucose transporters correlate to abnormal hyperphosphorylation of tau in Alzheimer disease, FEBS Lett. 582 (2008) 359–364.
[37] S. Förster, et al., Increased O-GlcNAc levels correlate with decreased O-GlcNAcase levels in Alzheimer disease brain, Biochim. Biophys. Acta 1842 (2014) 1333–1339.
[38] F. Liu, K. Iqbal, I. Grundke-Iqbal, G.W. Hart, C.-X. Gong, O-GlcNAcylation regulates phosphorylation of tau: a mechanism involved in Alzheimer's disease, Proc. Natl. Acad. Sci. 101 (2004) 10804–10809.
[39] R.R. Kalyani, J.M. Egan, Diabetes and altered glucose metabolism with aging, Endocrinol. Metab. Clin. North Am. 42 (2013) 333–347.
[40] N. Fülöp, et al., Aging leads to increased levels of protein O-linked N-acetylglucosamine in heart, aorta, brain and skeletal muscle in Brown-Norway rats, Biogerontology 9 (2008) 139–151.
[41] S. Liu, H. Sheng, Z. Yu, W. Paschen, W. Yang, O-linked β-N-acetylglucosamine modification of proteins is activated in post-ischemic brains of young but not aged mice: implications for impaired functional recovery from ischemic stress, J. Cereb. Blood Flow Metab. 36 (2016) 393–398.
[42] M. Jiang, et al., XBP1 (X-box-binding Protein-1)-dependent O-GlcNAcylation is neuroprotective in ischemic stroke in young mice and its impairment in aged mice is rescued by Thiamet-G, Stroke 48 (2017) 1646–1654.
[43] A. Tramutola, et al., Proteomic identification of altered protein O-GlcNAcylation in a triple transgenic mouse model of Alzheimer's disease, Biochim. Biophys. Acta Mol. Basis Dis. (2018), https://doi.org/10.1016/j.bbadis.2018.07.017.
[44] S. Wang, et al., Quantitative proteomics identifies altered O-GlcNAcylation of structural, synaptic and memory-associated proteins in Alzheimer's disease, J. Pathol. 243 (2017) 78–88.
[45] Y.S. Chun, O.-H. Kwon, S. Chung, O-GlcNAcylation of amyloid-β precursor protein at threonine 576 residue regulates trafficking and processing, Biochem. Biophys. Res. Commun. (2017), https://doi.org/10.1016/j.bbrc.2017.06.067.
[46] Y.S. Chun, et al., O-GlcNAcylation promotes non-amyloidogenic processing of amyloid-β protein precursor via inhibition of endocytosis from the plasma membrane, J. Alzheimers Dis. 44 (2015) 261–275.
[47] L.S. Griffith, M. Mathes, B. Schmitz, Beta-amyloid precursor protein is modified with O-linked N-acetylglucosamine, J. Neurosci. Res. 41 (1995) 270–278.
[48] K.T. Jacobsen, K. Iverfeldt, O-GlcNAcylation increases non-amyloidogenic

processing of the amyloid-β precursor protein (APP), Biochem. Biophys. Res. Commun. 404 (2011).
[49] Y. Akimoto, et al., Localization of the O-GlcNAc transferase and O-GlcNAc-modified proteins in rat cerebellar cortex, Brain Res. 966 (2003) 194–205.
[50] K. Vosseller, O-linked N-acetylglucosamine proteomics of postsynaptic density preparations using lectin weak affinity chromatography and mass spectrometry, Mol. Cell. Proteomics 5 (2006) 923–934.
[51] M.-Y. Cha, et al., Mitochondrial ATP synthase activity is impaired by suppressed O-GlcNAcylation in Alzheimer's disease, Hum. Mol. Genet. 24 (2015) 6492–6504.
[52] E.P. Tan, et al., Altering O-linked Beta-N-acetylglucosamine cycling disrupts mitochondrial function, J. Biol. Chem. 289 (2014) 14719–14730.
[53] E.P. Tan, et al., Sustained O-GlcNAcylation reprograms mitochondrial function to regulate energy metabolism, J. Biol. Chem. 292 (2017) 14940–14962.
[54] J.L. Sacoman, R.Y. Dagda, A.R. Burnham-Marusich, R.K. Dagda, P.M. Berninsone, Mitochondrial O-GlcNAc transferase (mOGT) regulates mitochondrial structure, function, and survival in HeLa cells, J. Biol. Chem. 292 (2017) 4499–4518.
[55] S.A. Yuzwa, et al., A potent mechanism-inspired O-GlcNAcase inhibitor that blocks phosphorylation of tau in vivo, Nat. Chem. Biol. 4 (2008) 483–490.
[56] S.A. Yuzwa, A.H. Cheung, M. Okon, L.P. McIntosh, D.J. Vocadlo, O-GlcNAc modification of tau directly inhibits its aggregation without perturbing the conformational properties of tau monomers, J. Mol. Biol. 426 (2014) 1736–1752.
[57] S.A. Yuzwa, et al., Increasing O-GlcNAc slows neurodegeneration and stabilizes tau against aggregation, Nat. Chem. Biol. 8 (2012) 393–399.
[58] N.B. Hastings, et al., Inhibition of O-GlcNAcase leads to elevation of O-GlcNAc tau and reduction of tauopathy and cerebrospinal fluid tau in rTg4510 mice, Mol. Neurodegener. 12 (39) (2017).
[59] S.A. Yuzwa, et al., Pharmacological inhibition of O-GlcNAcase (OGA) prevents cognitive decline and amyloid plaque formation in bigenic tau/APP mutant mice, Mol. Neurodegener. 9 (2014) 42.
[60] C. Kim, et al., O-linked β-N-acetylglucosaminidase inhibitor attenuates β-amyloid plaque and rescues memory impairment, Neurobiol. Aging 34 (2013) 275–285.